Dynamic Processes Permitting Stable Coexistence of Antimicrobial Resistant and Non-Resistant Organisms in a Gastrointestinal Tract Model

Tippawan Puttasontiphot[a], Yongwimon Lenbury[a]*, Chontita Rattanakul[a], Sahattaya Rattanamongkonkul[b], John R. Hotchkiss[c] and Philip S. Crooke[d]

[a] Department of Mathematics, Faculty of Science, Mahidol University, Bangkok, 10400, Thailand.
[b] Department of Mathematics, Faculty of Science, Burapha University, Chonburi, 20131, Thailand.
[c] Department of Critical Care Medicine, University of Pittsburgh, Pittsburgh, PA 15261, USA.
[d] Biomathematics Study Group, Department of Mathematics, Vanderbilt University, Nashville, TN 37240, USA.

* Corresponding author, E-mail: scylb@mahidol.ac.th

ABSTRACT: In this paper, bacteria-antibiotic dynamics in a gastrointestinal tract exposed to antimicrobial selection pressure is modeled as occurring in a continuous chemostat. Two populations of microorganisms, one sensitive and the other resistant to an inhibitor, namely an antibiotic, compete for a single limiting resource. It is shown that conditions exist whereby the two types of bacteria can persist. Application of the singular perturbation analysis also yields delineating conditions on the "effective" antibiotic level that encode information on the minimum inhibitory concentration (MIC) and the minimum antibiotic concentration (MAC), which are extremely important parameters commonly used to quantify the activity of antibiotics against a given bacterium.

KEYWORDS: gastrointestinal tract model, antimicrobial resistance, continuous chemostat, singular perturbation.

INTRODUCTION

As has been noted by Nolting and Derendorf[1], "the outcome of treating bacterial infections with antibiotics is a function of multiple variables." Therapeutic efficacy depends on bacterial susceptibility to the antibiotics, specific properties of the infected site, metabolism in antibiotic elimination, dosing regimen, and several other factors. Up to date, many questions about dosing regimen remain unanswered[1]. Risk of infection may not be reduced even though the antibiotic dose is titrated to produce serum concentrations within the recommended range.

Parameters traditionally used to quantify the activity of antibiotic against bacterial infection are the minimum inhibitory concentration (MIC), the minimum bactericidal concentration (MBC) and the minimum antibiotic concentration (MAC). These parameters are determined under standardized conditions as discussed in Nolting and Derendorf's report[1]. There are several disadvantages to this approach, however. The *in vitro* models do not necessarily reflect the *in vivo* situation where the drug undergoes metabolism and elimination. The inoculum size can be variable and the infected size might pose severe restrictions on antibiotic diffusion into the tissue[1]. Most importantly, prolonged treatment can give rise to resistant strains. Such

concerns have prompted researchers to devise *in vitro* systems or models to simulate *in vivo* conditions and to investigate the killing effects of antibiotics against bacteria as a function of time.

The mammalian digestive tract becomes colonized with bacteria acquired, since birth, from the mother and the immediate environment. Numerous bacterial species populate the digestive tract and constitute the indigeneous gastrointestinal flora of a mammal contributing to a gastrointestinal ecosystem that is necessary for an animal to digest and absorb nutrients efficiently from the alimentary[2]. It is well known that the gastrointestinal (GI) microflora that inhabit the digestive tract of mammals have a great influence on the host's physiology, intestinal anatomy and resistance to infectious diseases[3].

Several studies[4,5] have demonstrated that overgrowth of intestinal bacteria promotes their translocation from the GI tract to other organs. Such translocation of viable bacteria from the GI tract to the mesenteric lymph nodes and other organs is undoubtedly an initial step in the pathogenesis of many bacterial diseases[4]. It was also reported by Steffenand and Berg[5] that the extent of translocation of certain indigenous bacteria is directly related to their population levels in the GI tract.

Apparently, there is a great variety in the

composition of gastrointestinal microflora among animals, as well as varying degrees of sensitivity among the microbials to the various antibiotics that might be used to inhibit their growth. However, the emergence of resistant microorganisms is always a potential risk when antibiotics are administered.

Moreover, a recent report[6] indicated that there is huge potential for genetic exchange to occur within the dense, diverse anaerobic microbial population inhabiting the GI tract of humans and animals. Specifically, Scott[6] reported on recent evidence that anaerobic bacteria native to the rumen or hindgut harbour both novel antibiotic resistance genes and novel conjugative transposons (CTns). These CTns, and previously characterized CTns, can be transferred to a wide range of commensal bacteria under laboratory and *in vivo* conditions.

In their investigation of the impact of various antibiotics on the fecal flora of newborn infants, Bennet et al.[7] found that sequential development of the neonatal intestinal flora can be dramatically altered upon administration of broad-spectrum antimicrobial agents. It takes possibly several weeks for the intestinal flora to return to normal even when administration of the antimicrobial agents was discontinued.

Additional evidence that demonstrates the importance of intestinal flora in the control of GI overgrowth was given in the work of Burr and Sugiyama[8], where it was shown that adult mice with normal microbial flora but treated with large oral doses of two broad spectrum antimicrobial agents are at least 50-fold more susceptible to *C. botulinum* intestinal colonization than untreated mice. The increased susceptibility of antimicrobial treated mice to *C. botulinum* intestinal colonization is terminated when the antibiotics are stopped and the mice are housed with untreated control mice.

A body of evidence[9] suggests that multiple mechanisms are employed by the flora to exclude non-indigenous organisms from the intestinal tract and to maintain the status quo. Only the most extreme stress situations, such as antibiotic administration, have major effects on the stability of the initial flora. Experiments of Freter et al.[10] provided data on possible *E. coli* population control mechanisms. Anaerobic continuous flow cultures of homogenates of intestinal contents from conventional mice mixed with *E. coli* in veal infusion broth suppressed *E. coli* population growth, compared with pure continuous flow cultures of *E. coli*. The inhibition of *E. coli* multiplication was reversed, however, by addition of glucose. These results suggested that competition for nutrients is the overriding activity of importance in the control of *E. coli* population growth in continuous flow cultures that reflect the intestinal conditions[10].

Thus, in this paper, the effects of antimicrobial selection pressure on bacterial population dynamics and competition in the gastrointestinal tract is modeled as occurring within a continuous chemostat. Two populations of microorganisms in the culture compete for a single limiting resource in the presence of a drug, or antibiotic, as the inhibitor to which one population is sensitive and the other resistant. Clinical data are utilized to support the choice of terms that appear in the model. We then investigate the conditions under which different dynamic behavior is possible. Through our analysis, different dosing and kill curves may be examined. The analytical results are discussed in terms of their clinical implications, in the hope that deeper insights may be gained which are important for the understanding of the stability of the microflora composition in the GI tract, as well as the possible factors that may disrupt such stability.

Model Construction

We visualize the gastrointestinal tract as a continuous flow chemostat in which C is the concentration of the resource, S the number of sensitive microbial population, R that of the resistant population, and A is the drug concentration at any moment in time. Resource enters the habitat at concentration C_1, while A_1 is the asymptotic antibiotic concentration. Sensitive and resistant populations are removed at the rates ω_1 and ω_2 while the resource and antibiotics are removed at the rates ω_3 and ω_4, respectively.

Experimental data have been collected from a culture of *Enterococcus faecalis* ATCC 29212 and *Serratia marcescens* ATCC 43861 growing in 1% Mueller-Hinton Broth II in the absence of antibiotics. The experimentally measured values of the microbial counts are then plotted, in Figure 1, against those obtained from the simulation of the following logistic model for the microbial population $X(t)$:
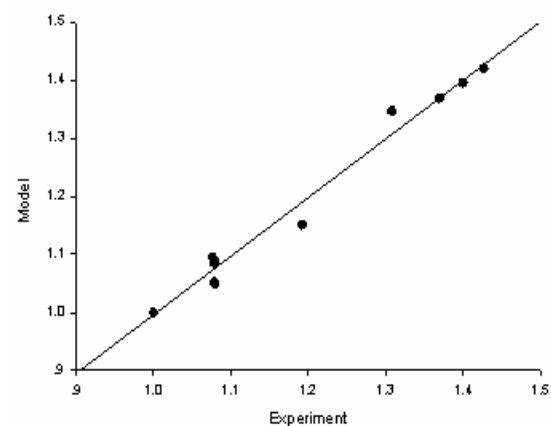

Fig 1. Plot of experimental data against model simulations.

$$\frac{dX}{dt} = \mu(C)\left(1 - \frac{X}{X_{max}}\right)X, X(0) = X_0 \qquad (1)$$

where $\qquad \mu(C) = \frac{\mu_{max}C}{K_S + C}. \qquad (2)$

We observe in Figure 1 that the data points are aligned along the straight line $y = x$. Experimenting with other sets of data yields the same result which assures us that the equation (1) gives a reasonable fit to the real data, with appropriately chosen values of the parameters.

Next, we incorporated antibiotic effect with the following model equation:

$$\frac{dX}{dt} = \mu_{max}\left(1 - \frac{X}{X_{max}}\right)X - \frac{\varepsilon_k AX}{K_K + A}, X(0) = X_0 \quad (3)$$

where $\qquad A(t) = A_1 + A_2 e^{-\omega t} \qquad (4)$

Figure 2 shows a comparison of the simulation of equation (3) with a set of experimental data collected from a culture of *Bacteroides Fragilis* (BF) with BMS-284756, an experimental drug, for the antibiotic, in Mueller-Hinton Broth II. The colony counts were done at $t = 0, 2, 4, 6, 8, 24$ and 48 hours by serial dilution in normal sterile saline. The parametric values, given in the figure caption, have been determined to obtain the best least square fit of the kill curve. A very close fit of this set of experimental data was obtained when the values of the parameters were suitably chosen.

Guided by the above observations and the discussion in the previous section, we will therefore consider the following model system of 4 ordinary differential equations.
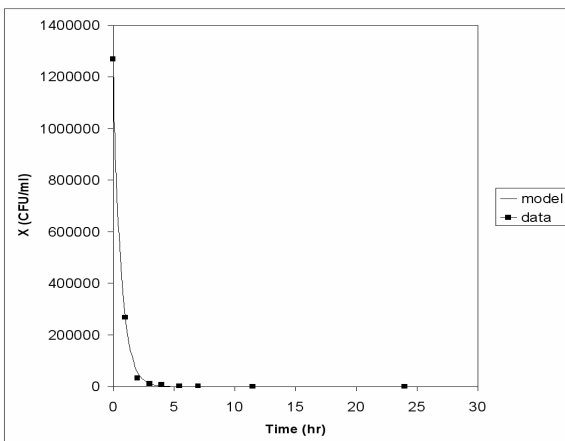

Fig 2. Comparison of numerical simulation. Data generated from equation (3), where $\mu_{max} = 0.02, X_{max} = 2.6 \times 10^6, \varepsilon_k = 1.5945848, K_K = 0.3911216, A_1 = 18.87638$ and $A_2 = 0.1, \omega = 0.9, X_0 = 1.27 \times 10^6$, was composed with a set of experimental data collected from a culture of *Bacteroides Fragilis* ATCC 25285 with BMS-284756 as the antibiotic in Mueller-Hinton Broth II grown on Tryptic-Soy agar plate.

$$\frac{dS}{dt_1} = \frac{\psi_S C}{(1 + \gamma_a A)(K_S + C)}(\gamma' - S)S$$
$$- \frac{\varepsilon_\gamma SR}{K_\gamma + S} - \frac{\varepsilon_K AS}{K_K + A} - \omega_1 S, S(0) = S_0 \qquad (5)$$

$$\frac{dR}{dt_2} = \frac{\psi_R RC}{K_R + C} + \frac{\varepsilon_\gamma SR}{K_\gamma + S} - \omega_2 R, R(0) = R_0 \qquad (6)$$

$$\frac{dC}{dt_3} = (C_1 - C)\omega_3 - \frac{\varepsilon_S \psi_S SC}{(1 + \gamma_a A)(K_S + C)} - \frac{\varepsilon_R \psi_R RC}{(K_R + C)}, C(0) = C_0 \qquad (7)$$

$$\frac{dA}{dt_1} = (A_1 - A)\omega_4, A(0) = A_0 \qquad (8)$$

where the first term in equation (5) is the growth rate of the susceptible population level S, taking after equation (2) previously mentioned. The second term accounts for the reduction in the number of susceptible population level as its member is converted into a resistant strain due to the acquisition of an extra chromosomal element, or plasmid, from members of the resistant strain. Resistance can also be due to chromosomal mutation that renders the strain insensitive to the antibiotics[11]. The third term in equation (5) is the rate at which the susceptible bacteria is killed off by the antibiotic, taking the form suggested by equation (3). The last term is then the rate of removal of S by natural means. The response functions used in equations (5) and (6) are of the Holling's type generally assumed in many previous population models[1,12-17]. This means that the consumption rate increases as the level of nutrient increases but reaches a saturation point, beyond which rate of consumption cannot increase even if there were more nutrient available. Here, we do not take into account the detoxification of the antibiotic (viz chloramphenicol by enzymatic acetylation), assuming that this effect is negligently small. Thus, in equation (8), the antibiotic is removed naturally at the rate that is proportional to its amount A at any time t.

Equation (6) describes the rate of change of the resistant population level R growing at the rate given by the first term which assumes a Holling type saturating function of the substrate concentration C. To give it a different dynamics from that of the susceptible strain, since R is the resistant strain and thus not limited by its environment, the growth rate of R is allowed to increase with its number, not limited by its surrounding conditions as in the logistic growth rate. The second term in equation (6) accounts for the increase in R due to the development of resistance in the susceptible strain. It is then naturally removed at the rate $\omega_2 R$.

The levels of S, R and C are assumed here to vary with different time scales t_1, t_2 and t_3, respectively, as shall be explained in the next section. Equation (7) describes the rate of change of the resource or substrate C. The second term accounts for its consumption by the susceptible bacteria S, while the last term accounts for that by the resistant bacteria R. Since S is sensitive to the presence of antibiotic A, the consumption rate by S is reduced as A increases, and thus the factor $1+\gamma_a A$ in the denominator of this term.

Since equation (8) is autonomous and depends only on A, it can be easily solved for $A(t)$ which is found to eventually tend to A_1 as time progresses. We may therefore consider the above model in the event that A has reached the level A_1. We are thus reduced to only the 3 equations (5)-(7) for $t \geq t_0$, with A replaced by A_0 such that $S(t_0) = S_0$, $R(t_0) = R_0$ and $C(t_0) = C_0$.

Model Analysis

In order to analyze the model equations (5)-(8) by the singular perturbation method, we further make the following assumptions.

As S represents the sensitive bacterial population, it is reasonable that S should have the fastest dynamics, while the resistant strain should be more adaptable to the environment and less susceptible to destruction and hence more stable, changing at a slower rate, or has intermediate dynamics. The resource C may be kept abundant at more or less constant level and thus assumed to have the slowest dynamics. We therefore utilize two small scaling parameters ε and δ, and dimensionless variables and parameters defined as follows.

Letting $t_1 = t + t_0, t_2 = \varepsilon t + t_0, t_3 = \varepsilon\delta t + t_0, x(t) = \frac{S(t_1)}{S_0}$,

$y(t) = \frac{R(t_2)}{S_0}, z(t) = \frac{C(t_3)}{S_0}$, $z_1 = \frac{C_1}{S_0}, K_\gamma = \frac{K_\gamma}{S_0}, K_S = \frac{K_S}{S_0}, K_R = \frac{K_R}{S_0}, \gamma = \frac{\gamma}{S_0}$, and

$a_1 = \frac{\psi_S}{1+\gamma_a A_1}$, $a_2 = \frac{\varepsilon_K A_1}{K_K + A_1}$, $a_3 = \frac{\varepsilon_S \psi_S}{1+\gamma_a A_1}$, $a_4 = \varepsilon_R \psi_R$,   (9)

one is led to the following system.

$$\frac{dx}{dt} = f(x,y,z), x(0) = x_0 \tag{10}$$

$$\frac{dy}{dt} = \varepsilon g(x,y,z), y(0) = y_0 \tag{11}$$

$$\frac{dz}{dt} = \varepsilon\delta h(x,y,z), z(0) = z_0 \tag{12}$$

where

$$f(x,y,z) = \frac{a_1 xz(\gamma - x)}{K_S + z} - a_2 x - \frac{\varepsilon_\gamma xy}{K_\gamma + x} - \omega_1 x \tag{13}$$

$$g(x,y,z) = \frac{\psi_R yz}{K_R + z} + \frac{\varepsilon_\gamma xy}{K_\gamma + x} - \omega_2 y \tag{14}$$

$$h(x,y,z) = (z_1 - z)\omega_3 - \frac{a_3 xz}{K_S + z} - \frac{a_4 yz}{K_R + z} \tag{15}$$

Thus, for fixed x, y and z, the rate of change $\left|\frac{dz}{dt}\right|$ is $O(\varepsilon\delta)$, $\left|\frac{dy}{dt}\right|$ is $O(\varepsilon)$, while $\left|\frac{dx}{dt}\right| = O(1)$. This means that x has the fastest dynamics, y the intermediate, and z the slowest dynamics. We can then carry out a singular perturbation analysis on the model system (10)-(12) with (13)-(15) that involves purely geometric arguments. Such method of analysis has been developed by Muratori and Rinaldi[12], extended to 3-dimensional systems by Muratori[13]. Examples of its use may be found in the works of Muratori and Rinaldi[14], Lenbury and Likasiri[15] and Rattanakul et al.[16]. Through the identification of the shapes and locations in the phase space of the equilibrium manifolds where $f(x,y,z) = 0$, $g(x,y,z) = 0$ and $h(x,y,z) = 0$, conditions can be determined under which as time passes, the three state variables $x(t)$, $y(t)$ and $z(t)$ tend to the corresponding steady state values x_s, y_s and z_s, respectively, at which point $f(x_s, y_s, z_s) = g(x_s, y_s, z_s) = h(x_s, y_s, z_s) = 0$. The direction of the trajectories in the phase space is determined by considering the signs of $\dot{x}$, $\dot{y}$ and $\dot{z}$ in different regions in the (x,y,z) - space delineated by the equilibrium manifolds. We are particularly interested in the case where the wash-out steady state $(0,0,z_1)$ is stable and the bacteria populations are eradicated.

Since experimental data invariably show oscillatory behavior in the time series, as can be seen in Figure 3, we are also interested in the possibility that our model allows such behavior. The conditions under which this occurs are important for control purposes and yield insightful interpretations.
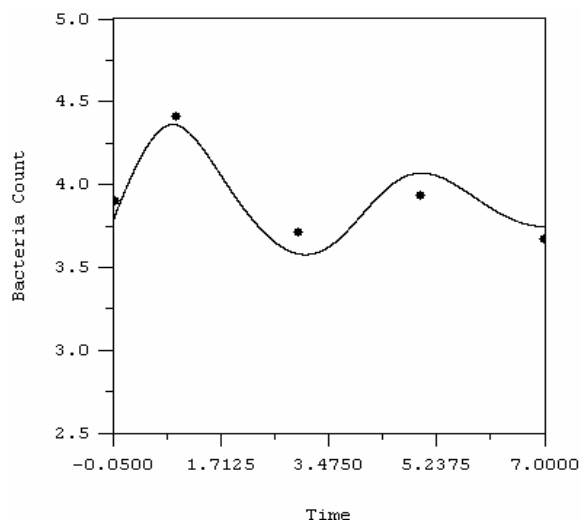

Fig 3. Colony counts of *Serratia marcescens* ATCC 43861 in varying concentration of 0.1% MHB with ceftazidime (0.125 ng/ml) on Trypticase-Soy agar plate. The colony counts were done at $t = 0, 1, 3, 5, 7$ hours by serial dilution in normal sterile saline. Experimental data are shown as dots, while the solid curve corresponds to the model simulation.

The shapes and relative positions of the manifolds $\{f = 0\}$, $\{g = 0\}$, and $\{h = 0\}$ determine the directions, speeds, and shapes of the resulting solution trajectories. Therefore, we need to analyze each of the equilibrium manifolds in detail. The delineating conditions for occurrence of different dynamic behavior as well as the existence of limit cycles are arrived at from the close inspection of those manifolds.

The manifold $\{f = 0\}$

This manifold consists of two submanifolds. One is the trivial manifold $x = 0$, while the other is the nontrivial manifold given by the equation

$$y = \frac{\left[a_1\gamma K_\gamma - (\omega_1 + a_2)K_\gamma\right]z - (\omega_1 + a_2)K_S K_\gamma}{\varepsilon_\gamma(K_S + z)}$$

$$+ \frac{\left[a_1(\gamma - K_\gamma) - (\omega_1 + a_2)\right]z - (\omega_1 + a_2)K_S\big]x - a_1 z x^2}{\varepsilon_\gamma(K_S + z)} \quad (16)$$

The surface intersects the z-axis at the point where

$$z = \frac{(\omega_1 + a_2)K_S}{a_1\gamma - (\omega_1 + a_2)} \equiv z_2 \quad (17)$$

In order that $z_2 > 0$, we need to require

$$a_1\gamma > (\omega_1 + a_2) \quad (18)$$

Moreover, the curve where the surface intersects the (y, z)-plane is asymptotic to the line

$$y = \frac{a_1\gamma K_\gamma - (\omega_1 + a_2)K_\gamma}{\varepsilon_\gamma} \equiv y_1 \quad (19)$$

for which $y_1 > 0$ provided (18) holds. Also the curve where the surface intersects the (x, z)-plane is asymptotic to the line

$$x = \frac{a_1\gamma - (\omega_1 + a_2)}{a_1} \equiv x_1 \quad (20)$$
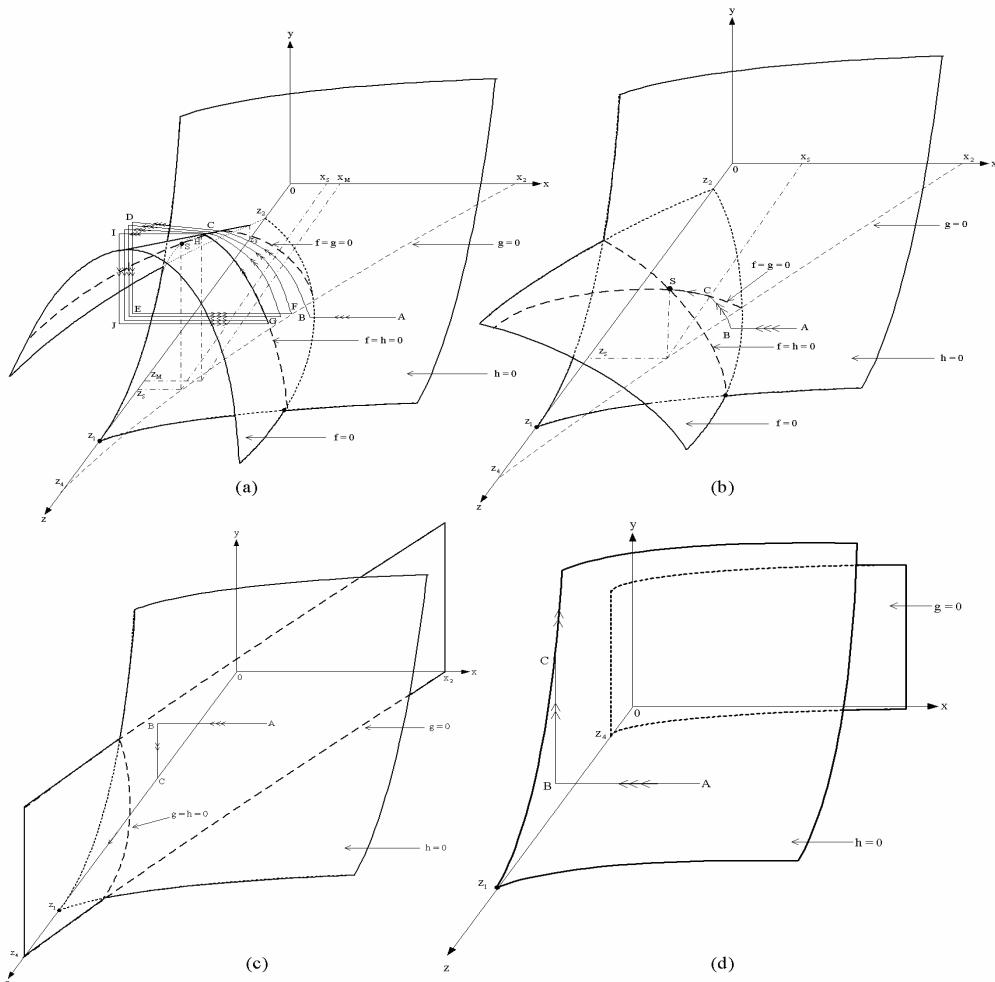
for which $x_1 > 0$ provided (18) holds.

Fig 4. Trajectories of the model system (10)-(12) with (13)-(15). The trajectory tends to a limit cycle in a), a positive equilibrium point in b), a wash-out equilibrium point in c), and becomes unbounded in d).

We now consider $\dfrac{\partial y}{\partial x}$, the slope of y given by (16) as a function of x, for a fixed z, as follows.

$$\frac{\partial y}{\partial x} = \frac{\left[a_1(\gamma - K_\gamma) - (\omega_1 + a_2)\right]z - (\omega_1 + a_2)K_S - 2a_1 xz}{\varepsilon_\gamma(K_S + z)} \quad (21)$$

We see that $\dfrac{\partial y}{\partial x} = 0$ along the curve where

$$x(z) = x_{max} = \frac{\left[a_1(\gamma - K_\gamma) - (\omega_1 + a_2)\right]z - (\omega_1 + a_2)K_S}{2a_1 z} \quad (22)$$

In order that $x_{max} > 0$, we need

$$z > \frac{(\omega_1 + a_2)K_S}{a_1(\gamma - K_\gamma) - (\omega_1 + a_2)} \equiv z_3 \quad (23)$$

We observe that $z_3 > 0$ if

$$a_1(\gamma - K_\gamma) > \omega_1 + a_2 \quad (24)$$

in which case the manifold $\{f = 0\}$ is shaped and located in the phase space shown in Figure 4a.

The manifold $\{g = 0\}$

This manifold consists of two submanifolds. One is the trivial manifold $y = 0$, while the other is the nontrivial manifold given by the equation

$$x = \frac{(\psi_R - \omega_2)K_\gamma z - \omega_2 K_R K_\gamma}{(\omega_2 - \psi_R - \varepsilon_\gamma)z + (\omega_2 - \varepsilon_\gamma)K_R} \quad (25)$$

This nontrivial manifold is independent of the intermediate variable y, and thus it is parallel to the y-axis. It intersects the z-axis at the point where

$$z = \frac{\omega_2 K_R}{\psi_R - \omega_2} \equiv z_4 \quad (26)$$

which will be positive if

$$\psi_R > \omega_2 \quad (27)$$

Moreover, it intersects the x-axis at the point where

$$x = \frac{\omega_2 K_\gamma}{\varepsilon_\gamma - \omega_2} \equiv x_2 \quad (28)$$

which will be positive if

$$\omega_2 < \varepsilon_\gamma \quad (29)$$

The manifold $\{h = 0\}$

This manifold is given by the equation

$$y = \frac{(z_1 - z)(K_S + z)(K_R + z)\omega_3 - a_3 xz(K_R + z)}{a_4 z(K_S + z)} \quad (30)$$

which intersects the z-axis ($x = y = 0$) at the point where

$$z = z_1 > 0 \quad (31)$$

We see that we need to require that

$$z_4 > z_1 \quad (32)$$

and

$$x_2 > x_1 \quad (33)$$

for the surfaces to be located as shown in Figures 4a-d.

We now let (x_S, y_S, z_S) be the intersection point of $\{f = 0\}$, $\{g = 0\}$ and $\{h = 0\}$, with $x_S > 0, y_S > 0, z_S > 0$, and let (x_M, y_M, z_M) be the maximum point of the curve $f = h = 0$. Four cases of different dynamic behavior can be identified as follows.

Case 1. This case is identified by the inequalities (18), (24), (27), (29), (32), (33), and $0 < x_S < x_M$.

Under these conditions, the shapes and relative positions of the equilibrium manifolds $\{f = 0\}$, $\{g = 0\}$ and $\{h = 0\}$ are as depicted in Figure 4a, where three arrows indicate fast transitions, two arrows indicate intermediate ones, while single arrows indicate slow ones.

Thus, a system initially at a generic point, say point A of Figure 4a, will make a quick transition to the surface given by equation (16) of the fast manifold $\{f = 0\}$ (point B in Figure 4a), since the signs of f assure us that this part of the manifold $\{f = 0\}$ is stable. As the surface where $\{f = 0\}$ is approached, y has slowly become active. A transition at an intermediate speed is made along $\{f = 0\}$ in the direction of increasing y, since $g > 0$ here.

Once the point C is reached, the stability of the manifold is lost, a catastrophic transition brings the system to point D on the (x,z)-plane. Consequently, the system will slowly develop along this plane in the direction of decreasing y, since g is now negative.

At a point E on the (y,z)-plane, the stability will again be lost and a quick transition will bring the system back to the point F which almost closes a cycle. However, since this part of the transition is in the region where $\dot{z} > 0$, z slowly increases giving rise to a high frequency oscillation which densely covers a surface, until the point H on the curve $\{f = h = 0\}$ is reached. A quick jump brings the trajectory to point I which is on the (y,z)-plane, and an intermediate transition will bring the system to the point J, followed by a quick transition which will bring the system back to the point G which lies on the stable part of the curve $\{f = h = 0\}$, thereby forming a closed cycle GHIJG. Thus, the existence of a limit cycle in the system for ε and δ sufficiently small is assured.

Case 2. This case is identified by inequalities (18), (27), (29), (31), (32) and (33) while (24) is violated (see Figure 4b).

Under these conditions, the system initially at a generic point A will make a quick transition to the fast manifold $\{f = 0\}$ (point B), then an intermediate transition is made along this surface in the direction of increasing

y until the curve $\{f = g = 0\}$ is reached. The trajectory will follow this curve until the stable equilibrium point (x_s, y_s, z_s) where $\{f = g = h = 0\}$ is reached at which point the transition ceases. This is, therefore, the case where all three populations persist at constant stable levels.

Case 3. This case is identified by inequalities (27), (29), (32), and (33) while (18), and thus (24), are violated. In Figure 4c, we see that the nontrivial fast manifold does not appear in the first octant since (18) does not hold. The intermediate manifold and the slow manifold are as shown in Figure 4c. A system initially at a point A, where the level of substrate C_0 is not too high, will make a quick transition to the trivial manifold $x = 0$, namely the (y,z)-plane (point B). Then, since $g < 0$ here, a transition at an intermediate speed in the direction of decreasing y is made to the point C on the

z-axis. Then the slow variable z has become active, and a transition at a slow speed is made along the z-axis to end at the stable equilibrium point $(0, 0, z_1)$. This is thus the case in which both susceptible and resistant bacterial populations are washed out.

Case 4. This case is identified by inequalities (27), (29), and (33), while (18), (24), and (32) are violated. Also, this is the case where $z_1 \gg z_4$ (high feed substrate or efficient substrate consumption by the resistant population). The system initially at a point A (in Figure 4d) will make a quick transition in the direction of decreasing x until a point B on the manifold $\{h = 0\}$ is reached (as shown in Figure 4d). At this point, the intermediate variable y has become active and a transition at intermediate speed is then made along $\{h = 0\}$ in the direction of increasing y, since $g > 0$ here in
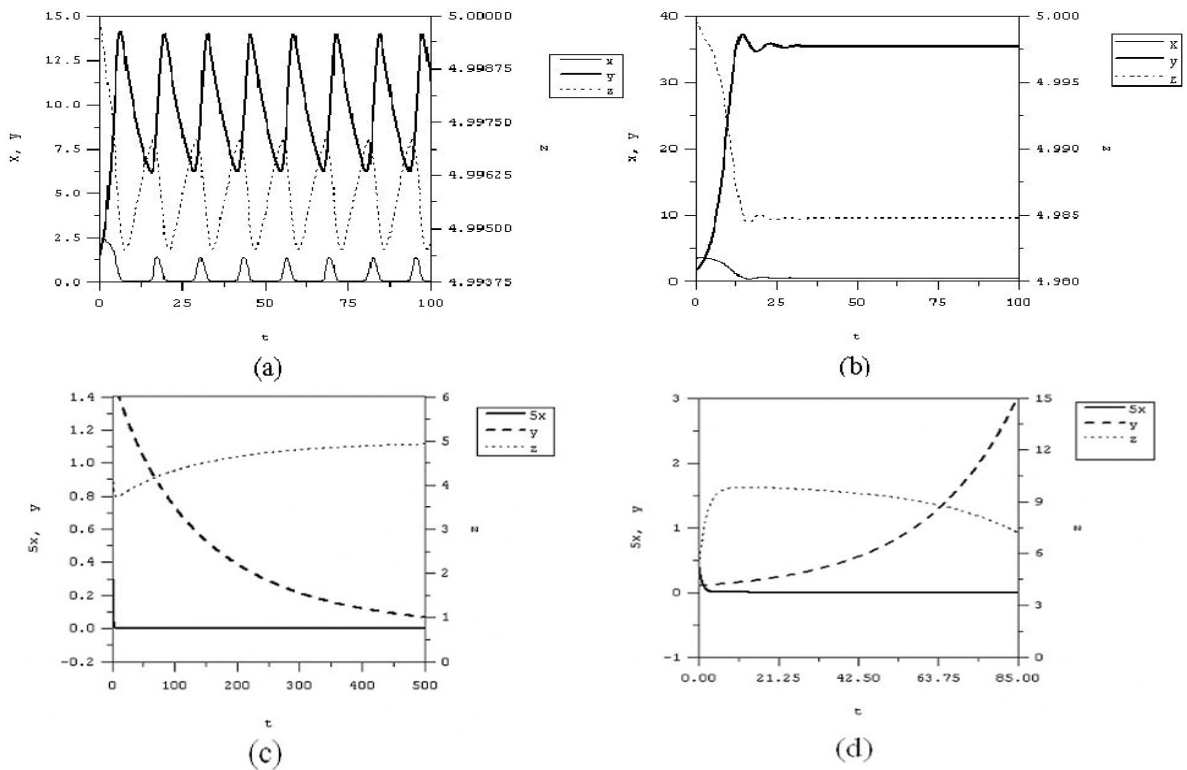

Fig 5. Time courses of x, y and z corresponding to the 4 cases of Figure 4.
(a) $\varepsilon = 1.0$, $\delta = 1.0$, $z_1 = 5.0$, $\varepsilon_\gamma = 0.9$, $\psi_R = 1.2$, $\gamma = 3.0$, $\omega_1 = 0.7$, $\omega_2 = 0.7$, $\omega_3 = 0.7$, $K_S = 0.7$, $K_\gamma = 1.5$, $K_R = 5.0$, $a_1 = 2.45283$, $a_2 = 0.023077$, $a_3 = 0.00196$, $a_4 = 0.0006$, $x_0 = 0.5$, $y_0 = 1.5$, and $z_0 = 5.0$. The solution in Case 1 exhibits sustained oscillation.
(b) $\varepsilon = 1.0$, $\delta = 1.0$, $z_1 = 5.0$, $\varepsilon_\gamma = 0.9$, $\psi_R = 1.2$, $\gamma = 4.0$, $\omega_1 = 0.7$, $\omega_2 = 0.7$, $\omega_3 = 0.7$, $K_S = 0.7$, $K_\gamma = 4.3$, $K_R = 5.0$, $a_1 = 2.407407$, $a_2 = 0.023077$, $a_3 = 0.00196$, $a_4 = 0.0006$, $x_0 = 0.5$, $y_0 = 1.5$, and $z_0 = 5.0$. The solution in Case 2 is seen here to tend towards a stable non-washout steady state values.
(c) $\varepsilon = 1.0$, $\delta = 1.0$, $z_1 = 5.0$, $\varepsilon_\gamma = 0.1$, $\psi_R = 0.09291$, $\gamma = 2.0$, $\omega_1 = 0.5$, $\omega_2 = 0.09$, $\omega_3 = 0.5$, $K_S = 2.0$, $K_\gamma = 2.0$, $K_R = 0.5$, $a_1 = 0.1$, $a_2 = 0.8$, $a_3 = 0.5$, $a_4 = 0.5$, $x_0 = 0.5$, $y_0 = 1.5$, and $z_0 = 5.0$. The solution in Case 3 is seen here to tend towards a stable wash-out steady state values.
(d) $\varepsilon = 1.0$, $\delta = 1.0$, $z_1 = 10.0$, $\varepsilon_\gamma = 0.06$, $\psi_R = 0.1$, $\gamma = 2.0$, $\omega_1 = 0.5$, $\omega_2 = 0.06$, $\omega_3 = 0.5$, $K_S = 2.0$, $K_\gamma = 2.0$, $K_R = 0.00001$, $a_1 = 0.1$, $a_2 = 0.8$, $a_3 = 0.5$, $a_4 = 0.5$, $x_0 = 0.1$, $y_0 = 0.1$, and $z_0 = 5.0$. The solution in Case 4 is seen here to exhibit a steady increase in the resistant population y.

front of the manifold $\{g = 0\}$, until the point C on the curve $\{h = 0\}$ on the plane $\{x = 0\}$ is reached. The transition will continue along this curve so that the resistant population can become too high leading to a bacteria overgrowth in the GI tract. The results of the above analysis may be stated as in the following theorem.

Theorem For the model system (10)-(12), with (13)-(15), and a suitable starting point (x_0, y_0, z_0), suppose inequalities (27), (29) and (33) hold.

1. If inequalities (18), (24) and (32) are satisfied and $0 < x_S < x_M$, then there exists a periodic solution to the model system which is locally asymptotically stable. The solution trajectory starting close enough to the unstable non-washout steady state (x_S, y_S, z_S) in this case will tend, as time progresses, towards a limit cycle which surrounds that steady state.

2. If the inequality (24) is violated, while (18) and (32) still hold, then the non-washout steady state will be stable. In this case, we have coexistence of the two microbial species at steady state levels.

3. If, moreover, (18) is violated (in which case (24) also is), while (32) still holds, then the washout steady state $(x, y, z) = (0, 0, z_1)$ is locally stable. In this case, there is an $\varepsilon_0 > 0$ such that if $C_0 < \varepsilon_0$, then bacteria are eventually eradicated.

4. On the other hand, when the environment is too conductive to bacteria growth, there exists a $\hat{C}$ such that if $C_0 > \hat{C}$ and (18), (24), and (32) are violated, with $z_1 >> z_4$, the mechanism to control the resistant strain through nutrient competition is no longer viable. The antibiotic dose of A_0 which settles down eventually to the level A_1 in this case is high enough to violate (24). The susceptible population is therefore quickly eliminated, allowing the overgrowth of the resistant population.

Numerical Simulation and Interpretation

Figure 5 shows the time series of the numerical simulations of model equations (10)-(12), with (13)-(15). The parameters are chosen to satisfy (18), (24), (27), (29), (32) and (33) in Figure 5a yielding a limit cycle solution as theoretically predicted. The solution trajectory in Figure 5b tends to the non-washout equilibrium point, while in Figure 5c it tends to the washout steady state $(0, 0, z_1)$ if it starts with a low C_0. However, if C_0 is too high bacteria overgrowth may be expected as shown in Figure 5d. We observe here that although our analysis was done on the assumption of ε and δ being small in order to carry out the singular perturbation arguments, our conclusions are in fact still valid even without ε or δ being very small. Both are set equal to 1 in the simulations shown in Figure 5.

In order to understand the clinical implications of the conditions given in the different cases of the above
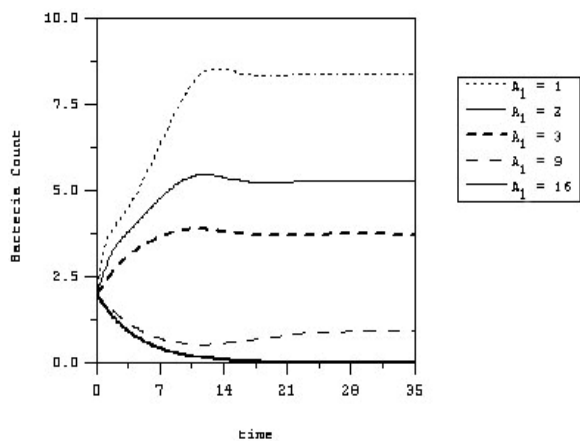

Fig 6. Kill curves for different "effective" antibiotic levels. $\varepsilon = 1.0$, $\delta = 1.0$, $z_1 = 5.0$, $\varepsilon_\gamma = 0.9$, $\psi_R = 0.5$, $\gamma' = 2.5$, $\gamma_a = 1.0$, $\omega_1 = 0.5$, $\omega_2 = 0.7$, $\omega_3 = 0.5$, $K_S = 2.0$, $K_\gamma = 2.0$, $K_R = 0.5$, $K_K = 1.0$, $\varepsilon_S = 0.000814$, $\varepsilon_R = 0.0006$, $\varepsilon_K = 0.046154$, $\psi_S = 4.814814$, $x_0 = 0.5$, $y_0 = 1.5$, $z_0 = 5.0$ and $S_0 = 1.0$, A_1 = antibiotic level.

theorem, we consider the delineating conditions (18) and (24). We define $\bar{a}_2$ as the value of a_2 that satisfies (18) when inequality is replaced by equality, namely,

$$\bar{a}_2 \equiv a_1 \gamma - \omega_1 \qquad (34)$$

and $\underline{a}_2$ as the value of a_2 that satisfies (24) when inequality is replaced by equality, namely,

$$\underline{a}_2 \equiv a_1 \gamma - \omega_1 - K_\gamma \qquad (35)$$

The above analytical conclusions may be understood to say that if the antibiotic dose can be kept at the sustaining level A_1, low enough so that the "inhibition factor" a_2 remains below the level $\bar{a}_2$, but kept high enough so that a_2 exceeds the critical level $\underline{a}_2$, then we shall be in Case 2 of the above theorem. That is, if

$$\underline{a}_2 < a_2 < \bar{a}_2 \qquad (36)$$

then the two bacterial populations can persist at controllable stable steady state levels (Case 2). However, if the antibiotic level asymptotically settles toward the level A_1 that is high enough so that the inhibition factor a_2 exceeds both $\bar{a}_2$ and $\underline{a}_2$, given in (34) and (35), then the inequalities (18) and (24) are both violated. We may then expect an eventual eradication of both the sensitive and the resistant populations (Case 3), provided that the initial condition (substrate level C_0) is not too highly conductive to bacteria growth.

Figure 6 shows different "kill curves" from our model simulations for different "effective" antibiotic levels A_1. The oscillatory behavior exhibited by our model in these kill curves closely resembles that

ScienceAsia 33 (2007)

205

observed in clinical data, an example of which is shown in Figure 3 where a simulation of our model is shown fitted with the experimental data, taking into account the measurement errors. Solving (34) for A_1 gives us an indication of the MAC (minimum antibiotic concentration), while solving (35) for A_1 provides a lower bound for the MIC (minimum inhibitory concentration). According to Sharma et al[18] the amount of time during which the antibacterial concentration remains above the MIC or MAC is an important determinant of deciding the dose regimens of an antibacterial agent.

However, the "effective" antibiotic level A_1 for each patient cannot be measured, but may by obtained by interpolating the pharmaco-kinetic data collected from controlled clinical trials. Considering equation (8), if the antibiotic rate of change of A is plotted against the antibiotic level A at each moment in time, then the slope of the fitted line that best fits the data shall give the value of ω_4, and the y-intersect of the line gives the value of $A_1\omega_4$, thus yielding the effective antibiotic level A_1 characteristic to each patient. In this way, it is possible to design the dosing regimen to obtain the desired outcome in the control range given by (36).

Finally, in terms of maintenance of the community stability in the GI tract, we can offer the following interpretation. The transition from a stable situation of Case 2 seen in Figure 5b to the unstable situation of Case 1 seen in Figure 5a occurs with the realization of condition (24). Considering this condition, we see that it may be satisfied with low enough antibiotic level A_1, or sufficiently low removal rate of susceptible population ω_1, or high enough carrying capacity γ of the environment for the susceptible population, or faster conversion of susceptible to resistant strain (low K_γ), or high enough initial nutrient level C_0.

Also, transition from the stable situation of Case 3 seen in Figure 6c to that seen in Figure 5d again is facilitated by the abundance of nutrients (large z_1) or efficient consumption of nutrients by the resistant population (high ψ_R or low K_R) so that $z_1 >> z_4$ even with a high level of antimicrobial agents A_1. Our model thus bears support to the experimental observation of Freter et al.[10], already mentioned in the Introduction, that suggested that competition for nutrients is of an overriding importance in the activity that maintains the stability of the microflora community. From such analysis, we can suggest a possible control strategy that combines appropriate drug protocol and strict diet regimen.

Conclusion

We have discussed a model of bacteria responses and resistance to antibiotics, which accounts for the mechanisms involved in the bacteria-antibiotic interactions *in vivo*. For a specific patient, it is possible to determine the values of the parameters by interpolating the data collected from controlled clinical trials, as has been described above. The model can then be used to simulate different dynamic behavior due to different dosing regimes. Since routine application of antibiotics inevitably leads to the emergence of drug resistance, it is vital that strategies are divised to reduce the speed with which this occurs.

Clinically, it is difficult to assess pharmaco-dynamic effects of antibiotics due to the complexity in repeatedly determining the bacterial load at the site of infection and antibiotic concentrations during the dosing interval[18]. Using dynamic models of bacteria-antibiotic interactions can overcome these difficulties. Through the model development and analysis, we gain an understanding of the pharmaco-dynamic factors that are involved in the process, while our model tries to simulate human infection mechanisms and can suggest how best the microbiological activity and antibacterial pharmacokinetic data *in vivo* can be used to select an antimicrobial agent and its dosage regimen that minimizes GI tract overgrowth by resistant species. The model might also be used to provide information regarding the kinetics of elimination of resistant strains once antimicrobial selection pressure has been relieved. Such information could prove useful in designing, monitoring, and control of empiric therapy stragies.

Acknowledgements

Appreciations are extended towards the Thailand Research Fund and National Center for Genetic Engineering and Biotechnology, National Science and Technology Development Agency (contract no. 3-2548) for financial support.

References

1. Nolting and Derendorf H (1995) Pharmacokinetic/ Pharmacodynamic Modeling of Antibiotics. CRC Press.
2. Johnson SA, Nicolson SW and Jackson S (2004) The effect of different oral antibiotics on the gastrointestinal microflora of a wild rodent (Aethomys namaquensis). *Comparative Biochemistry and Physiology*, **A138**, pp 475-83.
3. Tannock GW (1999) Medical importance of the normal microflora. Kluwer Academic Publ., Dordrecht, the Netherlands,.
4. Van der Waaij D, Berghuis-deVries JM and Lekkerkerk-van der Wees JEC (1972) Colonization resistance of the digestive tract and the spread of bacteria to the lymphatic organs in mice. *J. Hyg.* **70,** pp 335-42.
5. Steffenand EK and Berg RD (1983) Relationship between cecal population levels of indigenous bacteria and translocation to the mesenteric lymph nodes. *Infection and Immunity* **39(3)**, pp 1252-9.
6. Scott KP (2002) The role of conjugative transposons in

spreading antibiotic resistance between bacteria that inhabit the gastrointestinal tract. *Cell. Mol. Life Sci.* **59,** pp 2071-82.

7. Bennet R, Erickssen M, Nord CE and Zetterstrom R (1984) Impact of various antibiotics on the fecal flora of newborn infants. *Microecol. Ther.* **14**, pp 251.

8. Burr DH and Sugiyama H (1982) Susceptibility to enteric botulinum colonization of antibiotic-treated adult mice. *Infect. Immun.* **36,** pp103-6.

9. Van der Waaij D, Heidt PJ, Rusch VC and Gebbers JO (1990) Microbial ecology of the human digestive tract. In: *Old Herborn University seminar monograph,* pp 1-83. Institute for Microecology, Germany.

10. Freter R, Abrams GD and Aranki A (1973) Patterns of interaction in gnotobiotic mice among bacteria of a synthetic "normal" intestinal flora. In: *Germfree Research: Biological effect of gnotobiotic environments* (Ed.: Heneghan, J.B.). pp 429-434. Academic Press, New York, London.

11. Peacock SJ, Mandal S and ICJW (2002) Bowler, Preventing Staphylococcus aureus infection in the renal unit. *Q J Med* **95**, pp 405-10.

12. Muratori S and Rinaldi S (2002) A separation condition for the existence of limit cycles in slow-fast systems. International report, *Elettronica* **3,** pp 90.

13. Muratori S (1991) An application of the saparation principle for detecting slow – fact limit cycle in three – dimensional system. *Appl. Math. Comput.* **43**, pp 1-18.

14. Muratori S and Rinaldi S (1992) Low – and high – frequency oscillations in three – dimensional food chain systems. *SIAM Journal on Applied Mathematics.* **52,** pp 1688-706.

15. Lenbury Y and Likasiri C (1994) Low-and high-frequency oscillations in a food chain where one of the competing species feeds on the other. *Math. Comp. Modelling.* **20,** pp 71-89.

16. Rattanakul C, Lenbury Y, Krishnamara N and Wollkind DJ (2003)Modeling of bone formation and resorption mediated by parathyroid hormone: response to estrogen/PTH therapy. *BioSystems* **70,** pp 55-72.

17. Leah EK (1988) Mathematical models in biology. Random House, New York.

18. Sharma KK, Sangraula H and Mediratta PK (2002) Some New Concepts in Antibacterial Drug Therapy. *Indian Journal of Pharmacology* **34**, pp 390-6.